Acta Oceanol. Sin., 2024, Vol. 43, No. 7, P. 15–25
https://doi.org/10.1007/s13131-023-2279-2
http://www.aosocean.com
E-mail: ocean2@hyxb.org.cn

Evaluation and projection of marine heatwaves in the South China Sea: insights from CMIP6 multi-model ensemble

Kai Liu[1], Kang Xu[2]*, Tongxin Han[2], Congwen Zhu[3], Nina Li[4], Anboyu Guo[1], Xiaolu Huang[5]

[1] National Marine Environmental Forecasting Center, Beijing 100081, China

[2] State Key Laboratory of Tropical Oceanography, South China Sea Institute of Oceanology, Chinese Academy of Sciences, Guangzhou 510301, China

[3] State Key Laboratory of Severe Weather, Chinese Academy of Meteorological Sciences, Beijing 100081, China

[4] National Meteorological Center, China Meteorological Administration, Beijing 100081, China

[5] Inner Mongolia Autonomous Region Meteorological Observatory, Huhhot 010051, China

Received 30 June 2023; accepted 9 October 2023

© Chinese Society for Oceanography and Springer-Verlag GmbH Germany, part of Springer Nature 2024

Abstract

This study evaluates the performance of 16 models sourced from the coupled model intercomparison project phase 6 (CMIP6) in simulating marine heatwaves (MHWs) in the South China Sea (SCS) during the historical period (1982–2014), and also investigates future changes in SCS MHWs based on simulations from three shared socioeconomic pathway (SSP) scenarios (SSP126, SSP245, and SSP585) using CMIP6 models. Results demonstrate that the CMIP6 models perform well in simulating the spatial-temporal distribution and intensity of SCS MHWs, with their multi-model ensemble (MME) results showing the best performance. The reasonable agreement between the observations and CMIP6 MME reveals that the increasing trends of SCS MHWs are attributed to the warming sea surface temperature trend. Under various SSP scenarios, the year 2040 emerges as pivotal juncture for future shifts in SCS MHWs, marked by distinct variations in changing rate and amplitudes. This is characterized by an accelerated decrease in MHWs frequency and a notably heightened increase in mean intensity, duration, and total days after 2040. Furthermore, the projection results for SCS MHWs suggest that the spatial pattern of MHWs remains consistent across future periods. However, the intensity shows higher consistency only during the near-term period (2021–2050), while notable inconsistencies are observed during the medium-term (2041–2070) and long-term (2071–2100) periods under the three SSP scenarios. During the near-term period, the SCS MHWs are characterized by moderate and strong events with high frequencies and relatively shorter durations. In contrast, during the medium-term period, MHWs are also characterized by moderate and strong events, but with longer-lasting and more intense events under the SSP245 and SSP585 scenarios. However, in the long-term period, extreme MHWs become the dominant feature under the SSP585 scenario, indicating a substantial intensification of SCS MHWs, effectively establishing a near-permanent state.

Key words: marine heatwaves, South China Sea, global warming, future projections, CMIP6

Citation: Liu Kai, Xu Kang, Han Tongxin, Zhu Congwen, Li Nina, Guo Anboyu, Huang Xiaolu. 2024. Evaluation and projection of marine heatwaves in the South China Sea: insights from CMIP6 multi-model ensemble. Acta Oceanologica Sinica, 43(7): 15–25, doi: 10.1007/s13131-023-2279-2

1 Introduction

Marine heatwaves (MHWs) are prolonged extreme oceanic warming sea surface temperature (SST) events (Pearce and Feng, 2013; Hobday et al., 2016), which can cause severe impacts on large-scale ecosystems, fisheries, and human activities, leading to subsequent socioeconomic consequences (Frölicher and Laufkötter, 2018; Oliver et al., 2018; Smale et al., 2019; Smith et al., 2021). In the past few decades, various MHWs have been extensively recorded from the surface to the subsurface on continental shelves and in the open ocean (Oliver et al., 2021). The underlying causes of these events are a combination of local oceanic and atmospheric processes, which involve anomalies in air-sea heat flux, shoaling of the mixed layer, horizontal heat advection, vertical heat transport associated with reduced mixing, as well as coastal upwelling or Ekman pumping (Holbrook et al., 2020). Additionally, the MHWs can be significantly influenced by large-scale climatic variabilities through remote atmospheric or oceanic teleconnections (Oliver et al., 2021), such as El Niño-Southern Oscillation (ENSO, Di Lorenzo and Mantua, 2016; Chen et al., 2021; Liu et al., 2022b), Indian Ocean Dipole (IOD, Xiao et al., 2020) and Pacific Decadal Oscillation (PDO, Holbrook et al., 2019). Therefore, understanding the characteristics, trends, and associated driving mechanisms of MHWs is crucial for predicting and mitigating their impacts on marine ecosystems and human

Foundation item: The National Natural Science Foundation of China under contract Nos 42275024 and 42105040; the Key R&D Program of China under contract No. 2022YFE0203500; the Guangdong Basic and Applied Basic Research Foundation under contract Nos 2023B1515020009 and 2024B1515040024; the Youth Innovation Promotion Association CAS under contract No. 2020340; the Special Fund of South China Sea Institute of Oceanology of the Chinese Academy of Sciences under contract No. SCSIO2023QY01; the Science and Technology Planning Project of Guangzhou under contract No. 2024A04J6275.
*Corresponding author, E-mail: xukang@scsio.ac.cn

activities.

The increased global SST anomalies (SSTAs) lead to longer-lasting, more frequent, extensive, and intense MHWs (Frölicher et al., 2018; Yao et al., 2022), which are reflected in the global-averaged MHWs frequency and duration increasing by 34% and 17%, respectively, from 1925 to 2016 (Oliver et al., 2018). Furthermore, the linear trend of MHWs in China's marginal seas is even stronger than the global average, especially in the SCS (Yao et al., 2020; Yao and Wang, 2021). The MHWs in the SCS have a substantial impact on the abundant fishery resources and coral reef ecosystems due to their disruption of the symbiotic relationship between corals and algae (Eakin et al., 2019; Hughes et al., 2017). For example, an extreme MHW in 2015 resulted in the death of more than 40% of the coral communities on the Dongsha Atoll in the SCS (Xiao et al., 2020). In summer 2020, a record-breaking and prolonged MHW in the SCS also caused a massive coral bleaching event (Feng et al., 2022; Han et al., 2023). The Ministry of Agriculture the People's Republic of China (2017) has revealed that China plans to construct 45 national marine ranching demonstration zones in the SCS by 2025, but the ecosystems and fishery resources might be at risk from the severe impacts of MHWs, with high SST and low dissolved oxygen. Hence, a comprehensive understanding of the future changes in SCS MHWs under global warming is crucial for protecting marine ecosystems and indispensable in the selection of suitable sites and construction of marine ranching in the SCS.

Coupled general circulation models (CGCMs) participating in the coupled model intercomparison project (CMIP) are effective tools for understanding the variabilities of MHWs and projecting their related future changes under global warming. Many previous studies revealed that the global average MHWs days are projected to increase by a factor of 16 and 23 for the global warming of +1.5℃ and +2.0℃ relative to preindustrial levels, respectively (Frölicher et al., 2018; Oliver et al., 2019; Hayashida et al., 2020). Moreover, more extreme MHWs would occur during the global warming of +3.5℃ at the end of 21st century, with a near-permanent MHWs state by the 2070s (Plecha and Soares, 2020; Qiu et al., 2021). The MHWs changes induced by global warming exhibit large spatial-temporal inhomogeneity, for example, the largest increasing trends of MHWs in the western South Atlantic are projected to occur during 2021–2050 (Costa and Rodrigues, 2021), and Yao et al. (2020) also pointed out that 2040 is a pivotal year for the change of MHWs in the marginal seas of China. Conversely, in the Northeast Pacific, the duration of long-lived MHWs reduces by 31.0% under low-warming scenarios during 2051–2100 (Tang et al., 2023). Therefore, the responses of regional MHWs to global warming deserve further study, especially the SCS that is an area with more frequent human activities and fragile ecological environment.

However, most of the state-of-the-art CMIP models suffer from some substantial biases in simulating the global (Oliver et al., 2019; Plecha and Soares, 2020; Qiu et al., 2021) and regional MHWs (Darmaraki et al., 2019; Plecha et al., 2021). For example, both the CMIP phase 5 (CMIP5) and phase 6 (CMIP6) models underestimate the frequency and intensity of MHWs, but overestimate the duration of MHWs (Qiu et al., 2021). Compared with the CMIP5 models, CMIP6 models have an overall improvement in simulating the global and regional MHWs (Darmaraki et al., 2019; Plecha et al., 2021; Qiu et al., 2021). Several studies have closely examined the future changes of MHWs in different regions, including the northwestern Pacific (Xue et al., 2023) and the SCS (Dong et al., 2023; Song et al., 2023), utilizing CMIP6 models. Dong et al. (2023) and Song et al. (2023) specifically concentrated on the future summer MHWs in the SCS. However, Dong et al. (2023) primarily focused on the spatial changes of cumulative MHW intensity under a low emission scenario, while Song et al. (2023) revealed the responses of summer MHWs to the enhanced Western Pacific Subtropical High, excluding consideration of the warming trend under the shared socioeconomic pathway (SSP) 585 scenario runs. There remains an urgent need to further emphasize the future changes of SCS MHWs in response to varying global warming levels during different future periods. Therefore, with an enhanced and detailed understanding of the changes in SCS MHWs, we can enhance the protection of coral reef ecosystems in the SCS and adopt more effectively strategies to address climate change.

Given the importance of the MHWs in the SCS, the present study seeks to assess the capability of CMIP6 models in simulating the metrics of SCS MHWs and to examine their model-projected changes. Based on the MHWs intensity, the MHWs are divided into four categories, e.g., the moderate, strong, severe, and extreme MHWs (Hobday et al., 2018). Thus, we also try to investigate how the different intensity-based MHWs response to global warming under various SSP scenarios during different future periods. The remainder of this paper is organized as follows. Data and methods are introduced in Section 2. Section 3 describes the evaluation of the SCS MHWs in the CMIP6 model simulations, as well as their future projected characteristics. Finally, a discussion and conclusion can be found in Section 4.

2 Data and methods

2.1 *Datasets*

The daily SST data with a high horizontal resolution of 0.25° × 0.25° is extracted from the National Oceanic and Atmospheric Administration (NOAA) optimum interpolation sea surface temperature (OISST version 2) dataset (Reynolds et al. 2007) for the period of 1982–2020, which is referred to as observations for simplicity. The historical runs and future projections are derived from 16 CMIP6 models (Eyring et al., 2016). Table 1 provides details on the model names, modeling holders, used ocean model names, horizontal resolutions, and number of vertical levels used in these 16 CMIP6 models (see also http://www-pcmdi.llnl.gov). Note that the multi-model ensemble mean results from the historical runs of the selected 16 models are consistent with findings from previous studies (Yao et al., 2020; Qiu et al., 2021; Xue et al., 2023), particularly regarding the MHWs metrics. Here, the SSP126, SSP245, and SSP585 scenarios from CMIP6 models are selected to represent low, medium, and high future emissions and associated warming levels (O'Neill et al., 2016). Global climate CMIP6 model SST datasets are collected for both the historical period (1982–2014) and future climate (2015–2100). The historical run from 1985 to 2014 is adopted as the baseline of current climate, while the SSP run from 2015 to 2100 is considered as a projection of future climate.

To investigate the different responses of the SCS MHWs to various global warming levels, the period of 2015–2100 under the three SSP scenarios is divided into three 30-year segments, which are the near-term period (2021–2050), medium-term period (2041–2070), and long-term period (2071–2100), respectively. All the model outputs and observational datasets are horizontally interpolated onto a uniform spatial grid of 1.0° × 1.0° before analysis.

2.2 *MHW definition*

Following the MHWs definition proposed by Hobday et al. (2016), a MHW is defined as a prolonged discrete anomalously

Table 1. The basic information for 16 CMIP6 models, including names, associated institutions and countries, and resolution of each model

Number	Model	Center	Country	Ocean model name	Horizontal resolution, vertical levels
1	ACCESS-CM2	CSIRO	Australia	MOM5	300 × 360, 50 levels
2	ACCESS-ESM1-5	CSIRO	Australia	MOM5	300 × 360, 50 levels
3	BCC-CSM2-MR	BCC	China	MOM4	232 × 360, 40 levels
4	CanESM5	CCCma	Canada	NEMO3.4.1	290 × 361, 45 levels
5	CESM2-WACCM	NCAR	USA	POP2	384 × 320, 60 levels
6	CMCC-CM2-SR5	CMCC	Italy	NEMO3.6	292 × 362, 50 levels
7	CNRM-CM6-1-HR	CNRM	France	NEMO3.6	1 050 × 1 442, 75 levels
8	CNRM-CM6-1	CNRM	France	NEMO3.6	294 × 362, 75 levels
9	CNRM-ESM2-1	CNRM	France	NEMO3.6	294 × 362, 75 levels
10	GFDL-ESM4	NOAA-GFDL	USA	GFDL-OM4p5	576 × 720, 75 levels
11	IPSL-CM6A-LR	IPSL	France	NEMO-OPA	332 × 362, 75 levels
12	MIROC6	MIROC	Japan	COCO4.9.1	256 × 360, 63 levels
13	MPI-ESM1-2-HR	MPI-M	Germany	MPIOM1.63	404 × 802, 40 levels
14	MPI-ESM1-2-LR	MPI-M	Germany	MPIOM1.63	220 × 256, 40 levels
15	NorESM2-LM	NCC	Norway	MICOM	360 × 384, 70 levels
16	NorESM2-MM	NCC	Norway	MICOM	360 × 384, 70 levels

Note: The full title of abbreviations of centers are listed as follows: Commonwealth Scientific and Industrial Research Organisation (CSIRO), Beijing Climate Centre (BCC), Canadian Centre for Climate Modelling and Analysis (CCCma), National Center for Atmospheric Research (NCAR), Centro Euro-Mediterraneo per I Cambiamenti Climatici (CMCC), Centre National de Recherches Météorologiques (CNRM), National Oceanic and Atmospheric Administration Geophysical Fluid Dynamics Laboratory (NOAA-GFDL), Institute of Pierre Simon Laplace (IPSL), Model for Interdisciplinary Research on Climate (MIROC), Max Planck Institute for Meteorology (MPI-M), and Norwegian Climate Centre (NCC).

warm event whenever the daily SST exceeds the seasonally varying 90th percentile for at least five consecutive days. Here the 90th percentile is calculated for each calendar day using daily SST data within an 11-d window centered on the data across the 30-year climatology period (1985–2014), and with the result smoothed by applying a 31-d moving average. Successive events with a break of less than 2 d are combined and identified as a single event. Noted that the threshold of 90th percentile is determined based on a common period of 1985–2014 among the observations, the historical runs and the three SSP scenarios in CMIP6 models. This purpose is to compare the characteristics of SCS MHWs changes under different future global warming scenarios with the differences in historical run.

For the quantification of MHWs characteristics, we consider the following four metrics: the number of MHWs (MHWN, the number of discrete events in each year), MHWs duration (MHWD, the average duration of MHWs in each year), MHWs intensity (MHWI, the average intensity of MHWs in each year), and total number of MHWs days (MHWT, the number of MHWs days in each year). The detailed definitions and formulas for the four MHW metrics are provided in Table 2. When considering the future changes of MHWs, we use the metrics of MHWs averaged over the SCS (0°–25°N, 100°–125°E).

Similar to the MHWs definition, the intensity-based MHW categories (Hobday et al., 2018), determined by the magnitude of the MHW-related SSTA relative to the climatological 90th percentile scaled by the difference between the 90th percentile (threshold) and climatology, are also used in present study. The continuous severity index is based on the following equation:

$$\text{Severity}=\frac{\text{SSTA}_{\text{MHW}}}{\text{SST}_{\text{thres}}-\text{SST}_{\text{clim}}}, \tag{1}$$

where SSTA_{MHW} is the SSTA for the maximum intensity of the MHW event relative to the climatological 90th percentile, $\text{SST}_{\text{thres}}$ is a threshold of the 30-year (1985–2014) seasonally varying 90th percentile, and SST_{clim} is the 30-year seasonally varying SST climatology. Thus, each event is classified as being a moderate ($1 \leqslant$ severity < 2), strong ($2 \leqslant$ Severity < 3), severe ($3 \leqslant$ Severity < 4), or extreme (Severity $\geqslant 4$) MHW.

2.3 *Metric evaluation of CMIP6 datasets*

Following the previous studies (Zhou et al., 2014; Sun et al., 2022), the relative root mean squared error (RMSE′) is used to assess the empirical reliability and the robustness of the CMIP6 models' performances. The RMSE′ can be calculated as the fol-

Table 2. The definition and formulas of MHWs indices

Index	Definition	Formula	Unit
MHWN	the total number of discrete MHWs in each year	$\text{MHWN} = N$	time
MHWI	the average intensity of MHWs in each year	$\text{MHWI} = \sum_{i=1}^{N}\sum_{j}^{D_i}(\text{SST}_{ij} - \text{SST}_{\text{clim}})/N$	℃
MHWD	the average duration of MHWs in each year	$\text{MHWD} = \sum_{i=1}^{N}(D_i)/N$	d
MHWT	the sum of MHWs days in each year	$\text{MHWT} = \sum_{i=1}^{N}(D_i)$	d

Note: N is the number of MHWs in each year, i represents one out of N MHWs in each year. D_i represents the duration of MHW_i. j indicates one day of D_i during each MHW, SST_{ij} represents the SST for day j during the MHW_i, and SST_{clim} is the 30-year seasonally varying SST climatology.

lowing equation:

$$\mathrm{RMSE}' = \frac{\mathrm{RMSE} - \mathrm{RMSE}_{\mathrm{median}}}{\mathrm{RMSE}_{\mathrm{median}}}, \tag{2}$$

where RMSE represents the root mean squared error of a single CMIP6 model, and $\mathrm{RMSE}_{\mathrm{median}}$ indicates the ensemble median of RMSEs for the 16 selected models. Negative (positive) RMSE′ demonstrates a better (worse) performance than the majority of the models.

Besides RMSE′, the interannual variability skill score (IVS, Gleckler et al., 2008; Yang et al., 2021) is also utilized to quantitatively evaluate the interannual variability of the CMIP6 models with respect to observations, which is defined by

$$\mathrm{IVS} = \left(\frac{\mathrm{STD_O}}{\mathrm{STD_M}} - \frac{\mathrm{STD_M}}{\mathrm{STD_O}}\right)^2, \tag{3}$$

where $\mathrm{STD_M}$ and $\mathrm{STD_O}$ are the standard deviations of the simulations and observations, respectively. IVS is a symmetric variability statistic that used to estimate the similarity of interannual variation between the simulations and observations, with a smaller value indicating a better simulation of interannual variability. In addition, the pattern correlation coefficient (COR) and the relative standard deviation (RSD; Sun et al., 2022) are also used to evaluate the simulations of pattern characteristics of MHWs in the SCS. RSD is the ratio of spatial standard deviation, which is measured by

$$\mathrm{RSD} = \frac{\mathrm{STD_{MP}}}{\mathrm{STD_{OP}}}, \tag{4}$$

where $\mathrm{STD_{MP}}$ and $\mathrm{STD_{OP}}$ are the pattern standard deviations of the simulations and observations, respectively. If a model simulation is close to the observation, then the RSD and COR value would be closer to 1.0.

3 Results

3.1 *Evaluation of the SCS MHWs in CMIP6 models*

3.1.1 *Spatial-temporal variation of the MHWs in the SCS*

Figure 1 illustrates the characteristics of SCS MHWs during the historical period of 1982–2014 from the observations and the multi-model ensemble (MME) mean results of CMIP6 models. The various metrics of the MHWs show the spatial non-uniformity across the SCS. The MHWN ranges from 1.5 to 3.3 time/a, with the more frequent center exceeding 2.7 times in the northern SCS (Fig. 1a). Similar to the MHWN, the spatial pattern of the MHWI is characterized by a decreased intensity from the northern SCS to southern SCS, with the strongest MHWs higher than +1.5℃/time in the continental shelf of the northern SCS and Beibu Gulf (Fig. 1b). Differ from MHWN and MHWI, the spatial distribution of the MHWD is centered in the central SCS, with the maximum duration exceeding 12 d/time (Fig. 1c). Since the MHWT is mainly affected by the MHWN and MHWD, the spatial pattern of MHWT is similar to their corresponding spatial distributions, with the largest MHWT values exceeding 33 d in the northwestern SCS (Fig. 1d). These spatial patterns of various SCS MH-

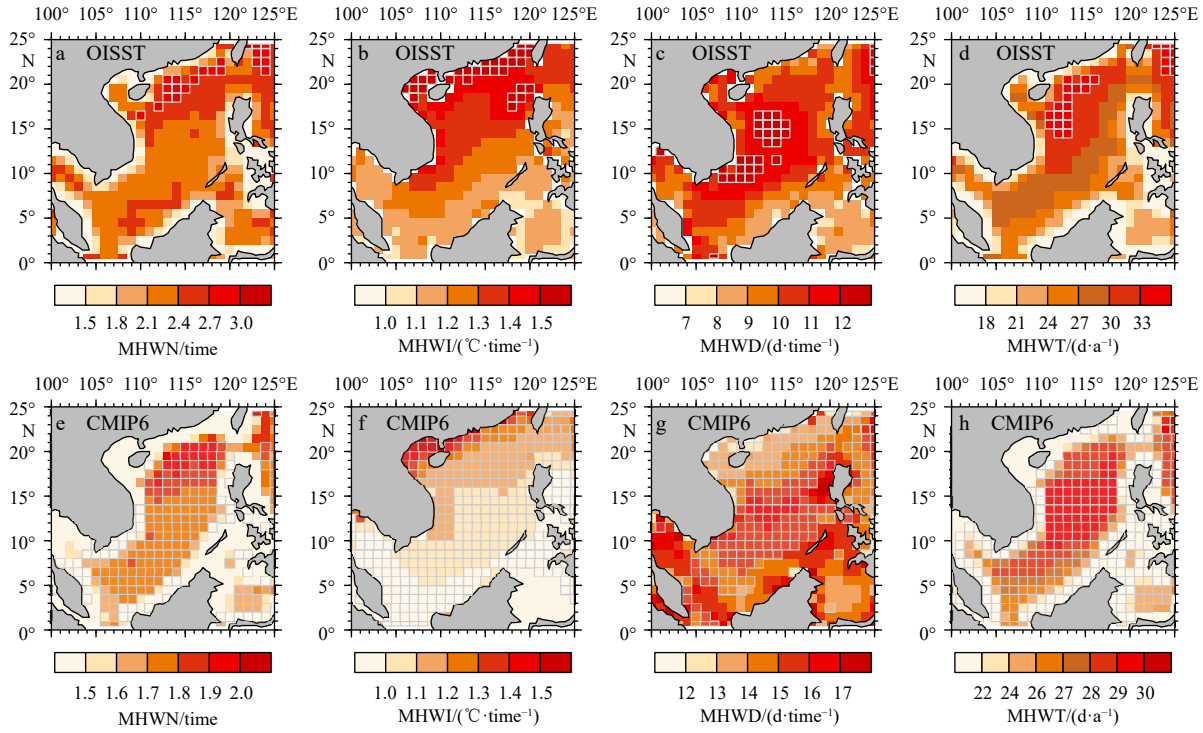

Fig. 1. Characteristics of the MHWs in the SCS during 1982–2014 from NOAA OISST data and the MME mean results based on the historical runs of the CMIP6 models. The spatial distributions of multiyear average number of MHWs (MHWN) (a), MHWs intensity (MHWI) (b), MHWs duration (MHWD) (c), and annual total number of MHWs days (MHWT) (d) in the SCS during 1982–2014 from OISST. The solid gray grid lines in Figs 1a–d represent the center exceeding 2.7 times,1.5 ℃/time, 12 d/time, and 33 d/a, respectively. Figs 1e–h are the same as Figs 1a–d, but for CMIP6 MME results, and the solid gray grid lines represent regions where the root mean squared error of the MME result is less than 20% relative to the observations.

Ws metrics are consistent with those reported by Yao et al. (2020), despite the different studying historical periods.

The simulation results of the 16 CMIP6 models in the historical runs clearly demonstrate a close resemblance of the MME mean for the SCS MHWs' metrics to the observed values. All the pattern correlations exceed +0.90, despite the different magnitudes of the simulated MHWs' metrics. The spatial patterns of the historically simulated MHWN and MHWI are quite similar to the observational counterparts, with the maximum values concentrated over the northern SCS but weaker corresponding amplitudes (Figs 1e and f), implying a slight underestimation of the SCS MHWs frequency and intensity in CMIP6 models. In contrast, the CMIP6 MME tends to overestimate the MHWD, despite the spatial patterns being similar between the historical simulations and observations (Fig. 1g). Furthermore, the CMIP6 MME also exhibits a slight underestimation of the MHWT, albeit with a minor error (Fig. 1h). Upon comparing the results with the global average (Qiu et al., 2021), it is evident that the CMIP6 models exhibit greater capability in reproducing observed SCS MHWs, and the associated biases are relatively smaller in magnitude. In most areas of the SCS, the RMSE of the MME result is less than 20% when compared to the observations (Figs 1e–h). This result indicates that CMIP6 models are capable of realistically simulating the intensity and spatial distribution of SCS MHWs in the historical runs, with more frequencies and warmer amplitudes of MHWs occurring over the northern SCS and longer durations concentrating in the central SCS.

To comprehensively evaluate the simulation performance of the SCS MHWs' metrics in the CMIP6 historical runs, we further present detailed statistical comparisons of the 16 selected models' simulations relative to the observations (Fig. 2, lighter colors represent better model performances). Statistical results demonstrate that all the models exhibit superior performance in simulating spatial distributions and variations of the SCS MHWs compared to the intensity and interannual variability of these events, with all the COR exceeding +0.70 and the RSD basically being close to 1.0. Most of CMIP6 models can also simulate the intensity and interannual variability of the SCS MHWs' metrics well, due to their RMSE′ values ranging from −0.4 to 0 and IVS values below +0.4. However, considerable variation in the simulation of various SCS MHWs metrics exists across the CMIP6 models. In detail, the CMIP6 MME results show the best reproduction of MHWN and MHWI, followed by MHWT, while the simulation of MHWD shows relatively poorer performance. The spatial distribution, intensity, and interannual variation of MHWN and MHWI are all well replicated by the CMIP6 MME results, but the intensity and interannual variation of MHWD and MHWT are not accurately captured, especially in the MIROC6, IPSL-CM6A-LR, CESM2-WACCM, ACCESS-ESM1-5 and ACCESS-CM2 models. The performance of simulating SCS MHWs also varies significantly across models, with the GFDL-ESM4, CNRM-ESM2-1, CNRM-CM6-1, CNRM-CM6-1-HR, and CMCC-CM2-SR5 models demonstrating the best overall simulation.

Overall, the ensemble median of CMIP6 models is superior to each single model in each respect, indicating that the ensemble median can realistically capture the characteristics of SCS MHWs in both historical runs and future projections. To reduce the uncertainties of the participating models to a great extent, the MME mean is therefore determined to represent the projected changes of the SCS MHWs under global warming in the following study.

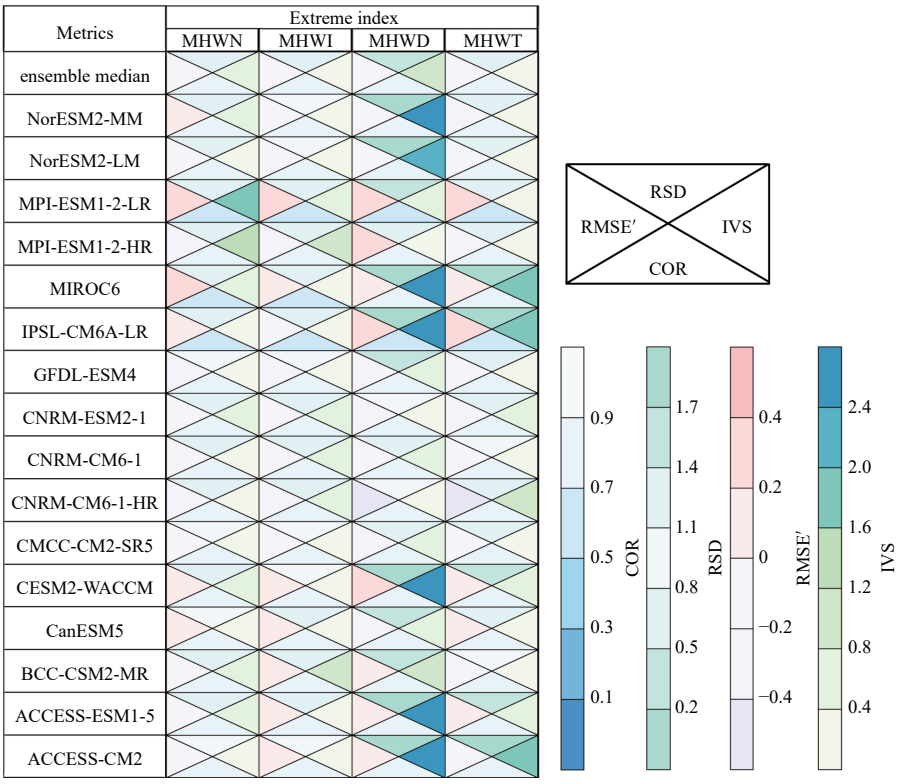

Fig. 2. Statistical metrics (MHWN, MHWI, MHWD, and MHWT) in the SCS MHWs based on the participating CMIP6 members versus the observations during the period of 1982–2014. COR is the pattern correlation coefficient, RSD is the ratio of standard deviation, RMSE′ is the relative root mean squared error and IVS is the interannual variability skill score.

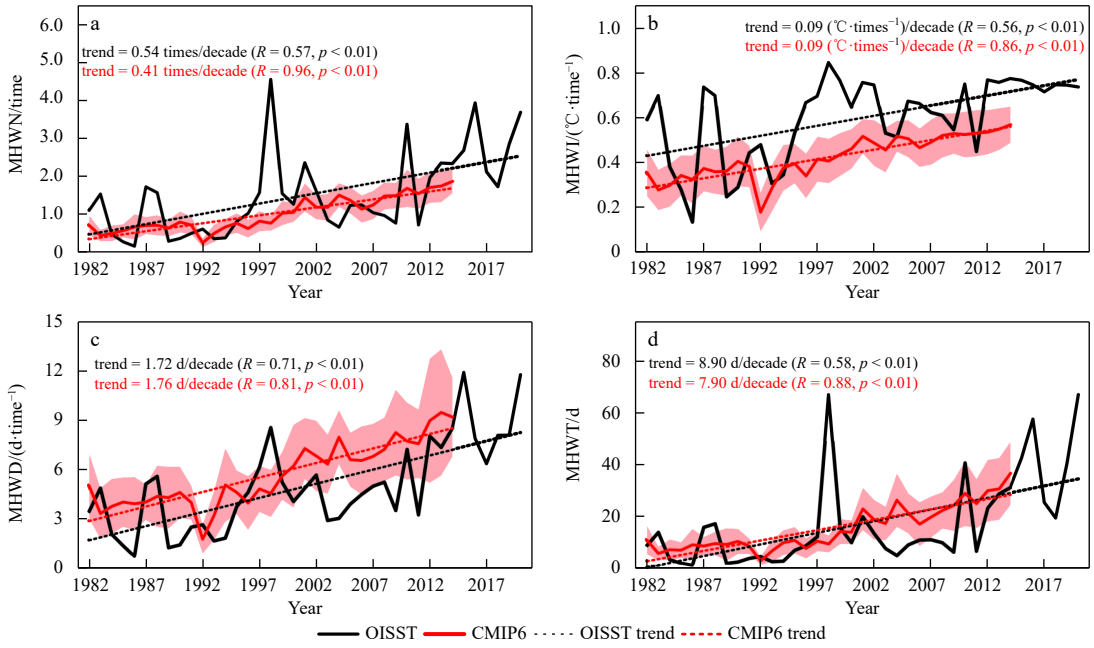

Fig. 3. Time series of the MHWN (a), MHWI (b), MHWD (c), and MHWT (d) averaged over the SCS (0°–25°N, 100°–125°E). The black (red) solid curves represent the results of the observations (the CMIP6 MME), and the black (red) dotted lines indicate the corresponding linear trends of the observations (the CMIP6 MME). The light red shadings denote the spread of 16 CMIP6 models included in the ensemble mean. The linear regression coefficients (trend), correlation coefficients (R), and associated significance of p-values are shown on the top in each panel.

3.1.2 *Trend variation of the SCS MHWs*

Observed results revealed that there existed a significant increase in the duration, intensity, coverage, and severity of summer MHWs in the SCS during 1982–2019, which can be primarily attributed to the SST warming trend (Tan et al., 2022). Hence, evaluating the performance of CMIP6 models in simulating the trends of the MHWs in the SCS and identifying the main drivers of these trends is a crucial aspect of the model evaluation process. Figure 3 shows the time series of the MHWs properties averaged over the SCS (0°–25°N, 100°–125°E) during the historical period. It is clearly seen that the CMIP6 models tend to underestimate the metrics of MHWN (Fig. 3a), MHWI (Fig. 3b), and MHWT (Fig. 3d), while overestimating the metric of MHWD (Fig. 3c). However, there exists a noticeably reasonable agreement between the CMIP6 modeled and observed SCS MHWs regarding the increasing trend during the historical period (Fig. 3). This suggests that CMIP6 models are able to reasonably reproduce the trends of SCS MHWs. During the historical period, the observed MHWN exhibited a growth rate of 0.54 time/decade, while the simulated MME MHWN displayed a slightly lower growth rate of 0.41 time/decade (Fig. 3a). For MHWI, both the observed and simulated MME showed an increasing amplitude of 0.09℃ per event per decade (Fig. 3b). Similarly, for MHWD, the observed and simulated MME exhibited an increasing trend of 1.72 d per event per decade and 1.76 d per event per decade, respectively (Fig. 3c). Additionally, the observed and simulated MME indicated a growth rate of 8.9 d/decade and 7.9 d/decade, respectively, for MHWT (Fig. 3d).

To examine the potential drivers of the trends of the SCS MHWs, the inter-model relationships between the trends of the MHWs and SSTA in the SCS for the historical period are presented in Fig. 4. The SCS SSTA trend of 0.183℃/decade, simulated by the CMIP6 MME, closely aligns with the observed SSTA trend of +0.18℃/decade from the OISST dataset. Furthermore, this SSTA trend is significantly correlated with the trend of simulated MHWs, with the intermodel correlation coefficients among all the CMIP6 models of +0.56, +0.78, +0.61, and +0.65, for MHWN, MHWI, MHWD, and MHWT, respectively. All these correlations are above the 95% significance level. This result indicates that CMIP6 models with larger SSTA trends are associated with increased frequent MHWs (Fig. 4a), higher intensity of MHWs (Fig. 4b), longer duration of MHWs (Fig. 4c), and more annual total days of MHWs (Fig. 4d) in the SCS. It is inferred that the warming SSTA trend is a significant driver of the SCS MHWs trend simulated by CMIP6 models.

To summarize, the CMIP6 MME results reasonably replicate the spatial-temporal variations of the SCS MHWs. Moreover, the MME simulated trends in SSTA and MHWs are closely related and in well accordance with the observations, suggesting that the increasing SSTA trend significantly influences various MHWs metrics. This underscores the reliability and scientific validity of employing CMIP6 MME results to project future changes in SCS MHWs.

3.2 *Future changes of the MHWs in the SCS*

Figure 5 illustrates the temporal evolution of the simulated characteristics of SCS MHWs, including both the historical runs and future SSP scenarios, relative to the period of 1985–2014. The projected changes of SCS MHWs vary depending on the low, medium, and high future scenarios and associated warming levels, with the decrease of MHWN and the increase of MHWI, MHWD, and MHWT at different rates. In detail, the MHWN in the SCS shows a rapid increase from 1982 to 2030, reaching peak values of 4.5 times to 5.0 times. However, after 2030, a gradual reduction is anticipated, reaching approximately 4.0 times and 2.5 times by the end of the 21st century under the SSP126 and SSP245 scenarios, respectively. Notably, after 2040, a dramatic decline is projected, dropping to around 1.0 time by the end of the 21st century

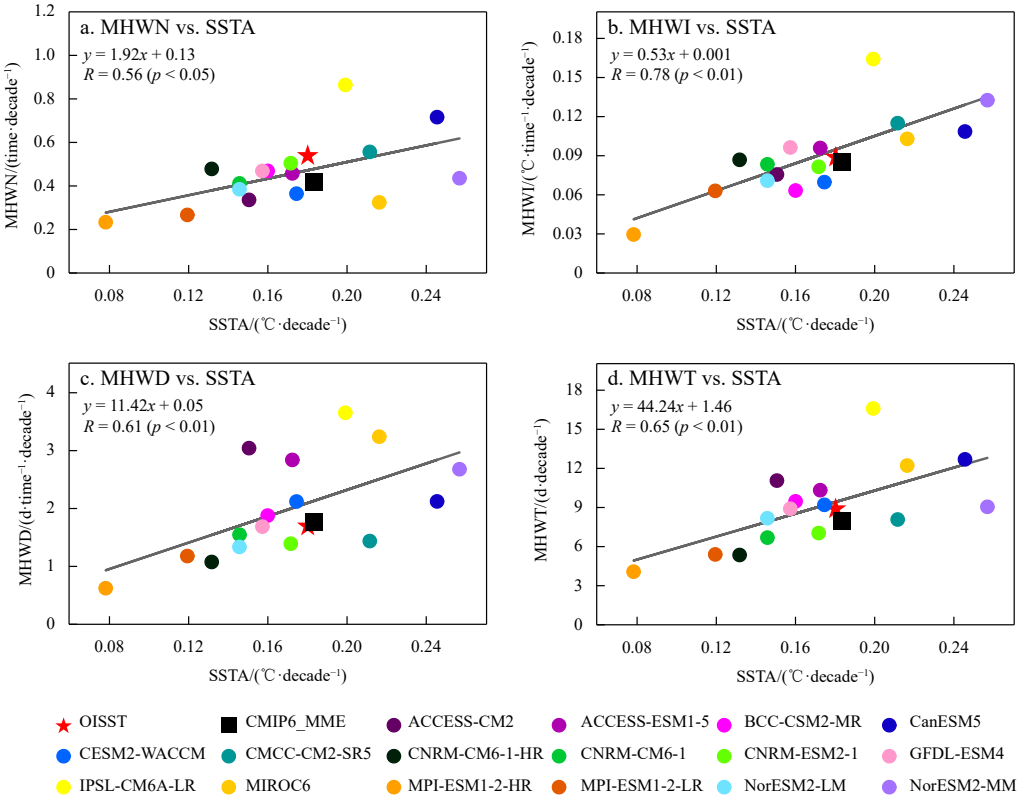

Fig. 4. Inter-model relationships of the CMIP6 models between the SSTA trend and the trend of the SCS MHWs. Scatterplots of the SCS SSTA trend vs. the SCS MHWN trend (a) , MHWI trend (b), MHWD trend (c), and MHWT trend (d). The colorful dots represent the results of 16 CMIP6 models, and the red star (black square) denotes the result of the observations (the CMIP6 MME). The black solid line denotes the best-fit line for the CMIP6 models based on linear regression, and the linear regression equation and its associated correlation coefficients, as well as the significance of *p*-values are shown on the left top of each panel.

under the SSP585 scenario (Fig. 5a). Regarding the intensity of SCS MHWs, the MHWI exhibits a slow increase under the SSP126 and SSP245 scenarios, peaking at just under +1.5℃ and +1.8℃ by the end of 21st century, respectively. In contrast, under the SSP585 scenario, after 2040, the MHWI experiences a rapid increase, reaching an apex of nearly +3.0℃ by the end of 21st century. This represents a threefold increase compared to the observed MHWI during the historical period (Fig. 5b). However, Song et al. (2023) emphasized that the summer SCS MHWI will exhibit slight changes at the end of 21st century when the linear warming trend of SST is removed even under the SSP585 scenario. Consequently, the changes in MHWI are affected by various global warming levels, regulating the amplitude of SCS SST warming trend.

The durations of SCS MHWs show an increasing trend, ranging from 90 d to 200 d under the SSP126 and SSP245 scenarios, respectively (Fig. 5c). The duration further extends to 365 d by the end of the 21st century, representing a near-permanent state of MHWs under the SSP585 scenario (Fig. 5c). Similarly, variations in the total days of SCS MHWs also exhibit an increasing trend, with a range of up to 200 d in SSP126 scenario, 300 d in SSP245 scenario, and 365 d in SSP585 scenario at the end of 21st century, respectively (Fig. 5d). While the MHWN starts to decrease after 2030, the rates of the decrease in MHWN and the increase in MHWI and MHWD during the 2030–2040 period are relatively gradual, and their magnitudes remain comparable across various SSP scenarios (Figs 5a–c). It is evident that after 2040, the decreasing trend of MHWN (Fig. 5a) accelerates, and the increasing trends in MHWI (Fig. 5b), MHWD (Fig. 5c), and MHWT (Fig. 5d) become more pronounced under different scenarios. Additionally, the amplitudes of these varying rates show a greater diversity in response to different levels of global warming. In other words, after 2040, the changing rates of MHWs under the SSP585 scenario are significantly stronger compared to those under the SSP126 and SSP245 scenarios. However, this distinction is not as pronounced before 2040. Therefore, the year 2040 serves as a crucial time point for the future changes of SCS MHWs under various SSP scenarios. This result is consistent with the future change of MHWs in the marginal seas of China revealed by Yao et al. (2020).

Analyzing the characteristics of SCS MHWs under the three SSP scenarios during the near-term period (2021–2051), medium-term period (2041–2070), and long-term period (2071–2100) can deepen our understanding of the future changes of SCS MHWs. This understanding can provide a scientific basis for proactive response to climate change and effective protection of marine ecosystems and fishery resources in the SCS. Figure 6 shows the boxplots that illustrates the projected SCS MHWs metrics during different future periods under the three SSP scenarios in CMIP6 models. It is clearly seen that the projection results exhibit higher consistency during the near-term period, while significant inconsistencies are observed during the medium-term and long-term periods under the three SSP scenarios. During the near-term period, the projected MHWN and MHWI is estimated to be approximately 4.5 times (Fig. 6a) and +1.1℃ (Fig. 6b) under all three SSP scenarios, but the influences of different SSP scenarios on SCS MHWs vary greatly during the medium-term and long-term periods. Taking the long-term period as an example, the MHWN under the SSP585 scenario is projected to be approx-

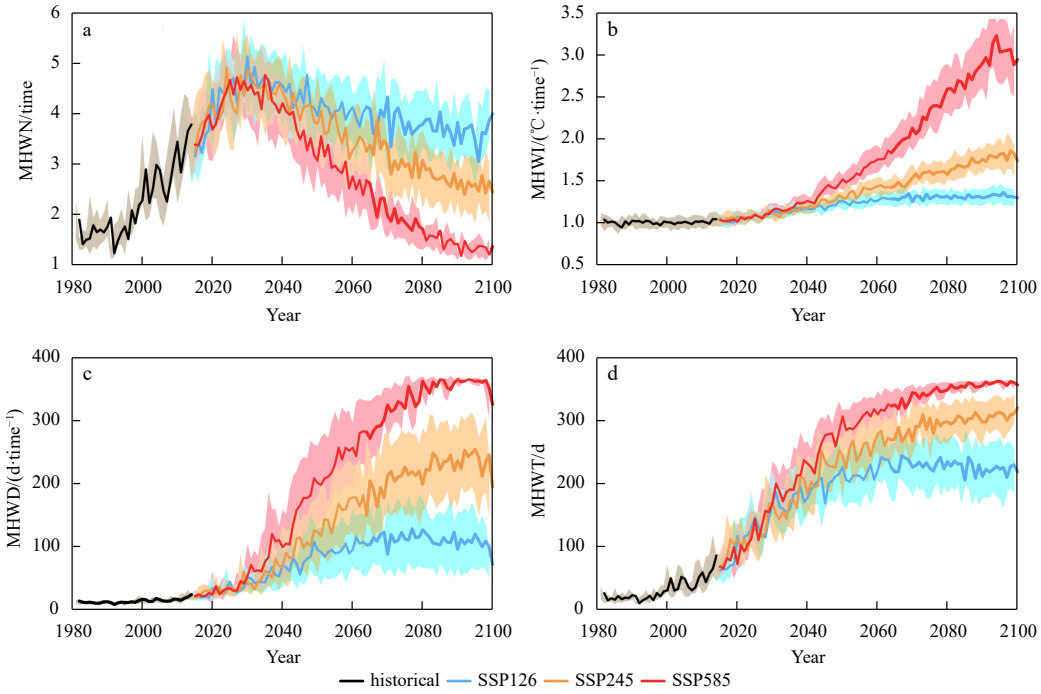

Fig. 5. Time series of the CMIP6 simulated SCS MHWs metrics from the historical and future (SSP) scenarios of global warming relative to 1985–2014. a. MHWN, b. MHWI, c. MHWD, and d. MHWT. The black, blue, orange, and red curves denote the MME results of the CMIP6 historical runs, SSP126, SSP245, and SSP585 scenarios, and the light black, blue, orange, and red shadings represent the corresponding spreads of CMIP6 models, respectively.

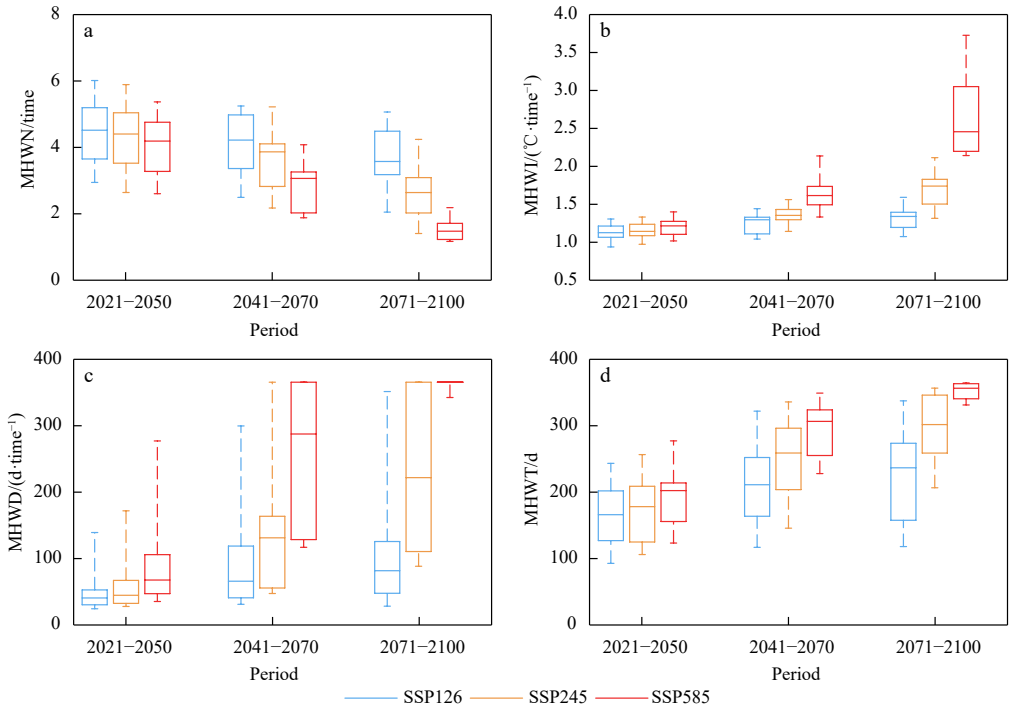

Fig. 6. Boxplots of the CMIP6 projected SCS MHWs metrics including MHWN (a), MHWI (b), MHWD (c), and MHWT (d) during the near-term period (2021–2050), medium-term period (2041–2070) , and long-term period (2071–2100) for different levels of global warming. The blue, orange, and red boxplots represent the results under the SSP126, SSP245, and SSP585 scenarios, respectively. The box-and-whisker plots show the minimum value, 25th percentile, median value, 75th percentile and maximum value of each metrics of MHWs.

imately 1.3 times lower than that under the SSP126 and SSP245 scenarios, respectively (Fig. 6a), and the MHWI under the SSP585 scenario is estimated to be +2.4℃, indicating that it is +1.1℃ and +0.7℃ stronger than that under the SSP126 and SSP245 scenarios, respectively (Fig. 6b).

Compared with the MHWN and MHWI, different SSP scenari-

os have greater impacts on MHWD and MHWT during the medium-term and long-term periods (Figs 6c and d). During the near-term period, the projected MHWD is estimated to range from 40 d to 60 d (Fig. 6c), while the MHWT is projected to be approximately 160 d to 200 d under the three SSP scenarios, respectively (Fig. 6d). During the medium-term period, there is a significant increase in the MHWD under the SSP245 and SSP585 scenarios, reaching 130 d and 280 d, respectively (Fig. 6c). A similar increase can be also observed in MHWT, reaching 260 d and 300 d by the end of 21st century under the SSP245 and SSP585 scenarios, respectively (Fig. 6d). During the long-term period, under the SSP245 scenario, the MHWD and MHWT are projected to reach 220 d (Fig. 6c) and 290 d (Fig. 6d), respectively. Furthermore, under the SSP585 scenario, both the MHWD and MHWT are expected to increase to be 365 d (Figs 6c and d), indicating a near-permanent state of MHWs throughout the year. As a result, the differences in the overall changes of SCS MHWs metrics' intensity among various SSP scenarios are significantly amplified during the medium-term and long-term periods compared to the near-term period. However, the patterns of the four MHWs' metrics remain consistent among various SSP scenarios during different future periods, with larger MHWN and MHWI concentrating in the northern SCS, while the longer MHWD and MHWT are located in the central and southern SCS (Figure not show). These results emphasize the need to provide well-informed recommendations regarding the location of marine pastures in the future, considering the growth rate and regional variations of MHWs, particularly in the South China coastal area and the southern SCS.

Next, we analyze the percentage of total days attributed to moderate, strong, severe, and extreme MHWs in the SCS using an intensity-based MHW categorization during the near-term, medium-term, and long-term periods under the three SSP scenarios (Fig. 7). The CMIP6 MME results in the historical runs show that the moderate MHWs days accounted for 78% of the total MHWs days, while the percentages of strong, severe, and extreme MHWs days were only 11%, 6%, and 5%, respectively (Figure not shown). During the near-term period, there is little difference in the SST warming amplitude caused by the three SSP scenarios. As a result, the percentages of moderate, strong, severe, and extreme MHWs days remain consistent across the three SSP scenarios and align with that observed in the historical period. Specifically, the moderate MHWs days are projected to be the most frequent, followed by the strong MHWs days, and the occurrences of severe and extreme MHWs are still expected to be low (Figs 7a, d, and g).

During the medium-term period, similar amplitudes of the SST warming, caused by the SSP126 and SSP245 scenarios, result in consistent percentages of the four types of MHWs days across both two scenarios (Figs 7b and e). However, under the SSP585 scenario, the percentage of moderate MHWs days is projected to decrease to 35.9%, which is approximately equal to the percentage of strong MHWs days at 34.6%. In this scenario, the percentages of severe and extreme MHWs days are estimated to increase to 19.1% and 10.4%, respectively (Fig. 7h). During the long-term period, the percentages of the four types of SCS MHWs days under the three SSP scenarios show significant differences. In par-

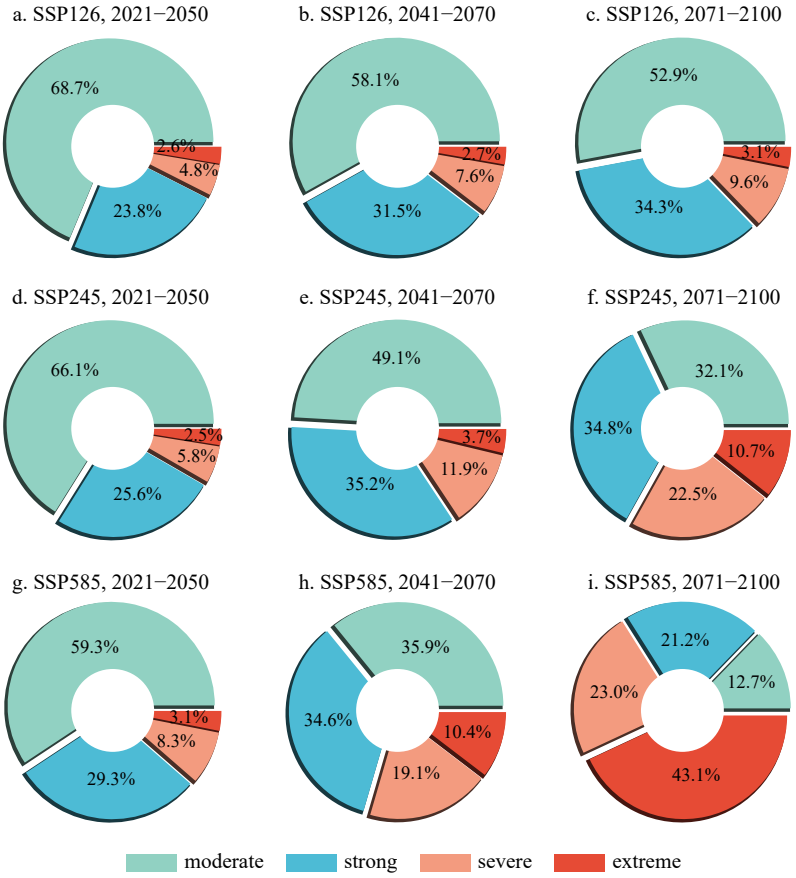

Fig. 7. Pie charts showing the total days of the moderate, strong, severe, and extreme SCS MHWs in percentage under the SSP126 (a–c), SSP245 (d–f) and SSP585 (g–h) scenarios. The left column (a, d, and g), middle column (b, e, and h) and right column (c, f, and i) represent the percentages during the near-term period (2021–2050) , medium-term period (2041–2070) and long-term period (2071–2100), respectively.

ticular, under the SSP245 scenario, the percentage of strong MHWs days is projected to be the highest, comprising 34.8% of the total MHWs days. Meanwhile, the percentage of moderate MHWs days is estimated to decrease to 32.1%, while severe MHWs days are expected to notably increase to 22.5% (Fig. 7f). Under the SSP585 scenario, the extreme MHWs days are projected to account for 43.1% of the total MHWs days, which is the highest percentage. Severe MHWs days follow with 22.5%, while the proportion of moderate MHWs days is estimated to be the lowest (Fig. 7i).

To sum up, the year 2040 is a crucial time point for the future changes of SCS MHW. Beyond this time, the changing rates of MHWs show substantial differences in response to various SSP scenarios. The decreasing trend in MHWN accelerates after 2040, while the increasing trends in MHWI, MHWD, and MHWT become more pronounced under the SSP585 scenario. Further analyses of the projected SCS MHWs metrics during different future periods under the three SSP scenarios suggest that, the change intensity of SCS MHWs during the near-term period show small differences across the three SSP scenarios, due to insignificant variations in warming levels caused by different scenarios. In contrast, during the medium-term and long-term periods, the warming effect varies among the scenarios, leading to substantial differences in the change intensity of SCS MHWs' metrics. However, the spatial patterns of the four MHWs' metrics remain consistent across the three future periods under the three SSP scenarios. During the medium-term period, MHWs are characterized by moderate and strong events, with longer-lasting and more intense under the SSP245 and SSP585 scenarios. However, during the long-term period, the SCS MHWs are mainly characterized by extreme events, with a near-permanent state under the SSP 585 scenario, implying a significant intensification of MHWs that is the prolonged and persistent occurrence throughout the year.

4 Conclusions and discussion

Despite intensive discussions on the changes in global and regional MHWs characteristics under a warmer climate, there is still much to learn about MHWs in the SCS and their associated changes in future climate. In this study, we evaluated the capability of CMIP6 models in simulating the key metrics of SCS MHWs during the historical period, and then discussed how future climate change might influence the SCS MHWs, with a particular emphasis on the future responses of the intensity-based MHWs across the near-term, medium-term, and long-term periods to the warmer climate under the three different SSP scenarios.

Results indicate that the majority of CMIP6 models exhibit a good capability in capturing the spatial-temporal distribution of SCS MHWs. These models successfully simulate the occurrence of MHWs with higher frequencies and warmer amplitudes predominantly along the South China coast, and also accurately reproduce longer MHWs durations that are primarily concentrated in the central SCS. There are certain limitations in the simulation of SCS MHWs, such as the underestimation of MHWN, MHWI, and MHWT, as well as the overestimation of MHWD, but the magnitudes of these model biases are relatively small compared to the global average. Despite these discrepancies, the CMIP6 models exhibit relatively good performance in capturing the overall characteristics of SCS MHWs, and their MME results perform best in capturing the characteristics of SCS MHWs. Further investigation into the linear trend of SCS MHWs during the historical period shows a reasonable agreement between the CMIP6 MME results and observations, indicating that the increasing trends of MHWs attributed to the warming SCS SSTA trend. These findings suggest that the projected changes in SCS MHWs based on CMIP6 model datasets are reliable and scientifically valid.

Regarding the future changes of SCS MHWs, it is noteworthy that the year 2040 serves as a pivotal time point when significant differences in changing rates emerge under various SSP scenarios. Furthermore, detailed analyses of the projected metrics of SCS MHWs and their classification into four categories during various future periods under the three SSP scenarios exhibit distinct differences. Specifically, during the near-term period, the characteristics of SCS MHWs exhibit a high level of consistency under the three SSP scenarios, and these MHWs are characterized by moderate and strong events with high frequencies and relatively shorter durations. However, as we move into the medium- and long-term periods, the warming effects of the three SSP scenarios exhibit variations, resulting in significant differences in the characteristics of SCS MHWs. During the medium-term period, the SCS MHWs are characterized by a combination of moderate and strong events, but there is a notable increase in severe and extreme events. Under the SSP245 and SSP585 scenarios, these events become longer-lasting and more intense. During the long-term period, the SCS MHWs predominantly exhibit extreme events, particularly under the SSP585 scenario. These extreme events persist for extended durations, leading to a near-permanent state of MHWs, which highlights a significant intensification of MHWs, with prolonged and persistent occurrences throughout the year.

The present results suggest that some models perform relatively poorer in simulating the interannual variation of SCS MHWD, which might be influenced by the factors such as ENSO (Yao and Wang, 2021; Liu et al., 2022b), intra-seasonal oscillation (ISO, Han et al., 2023) and other large-scale interannual modes (Xiao et al., 2020). Further investigations are thus required to identify the underlying sources of ENSO and ISO biases and uncertainties in CMIP6 models, to improve the models' ability to project future changes of SCS MHWs in the climate models. In addition, we have solely employed a stationary seasonal-varying threshold, derived from the 1985–2014 climate period, to estimate the future changes of SCS MHWs relative to the historical period and analyze their impacts on ecosystems that cannot adapt to rapid warming rates. However, the application of a non-stationary threshold, considering a moving climate period such as the research periods of 2041–2070 and 2071–2100 (Plecha et al., 2020), holds potential for further investigation. By utilizing a non-stationary threshold, the projections of SCS MHWs under the three SSP scenarios across the future periods would offer a more comprehensive understanding of their behavior and facilitating more accurate projections of their future trends. Furthermore, it is worth noting that our analysis only focused on the 90th percentile threshold for defining MHWs. However, considering higher thresholds such as the 95th and 99th percentiles (Frölicher et al., 2018) could provide a quantitative assessment of the ecological risks associated with SCS MHWs in the future. Last but not least, our projection results primarily rely on the MME results of 16 CMIP6 models, but the model biases might introduce uncertainties into the projections. Therefore, observationally constrained projection of MHWs in the SCS would be paid more attention in the future study, to reduce the spreads and uncertainties of the climate models.

References

Chen Ziyan, Shi Jian, Liu Qinyu, et al. 2021. A persistent and intense marine heatwave in the Northeast Pacific during 2019–2020. Geophysical Research Letters, 48(13): e2021GL093239, doi: 10.1029/2021GL093239

Costa N V, Rodrigues R R. 2021. Future summer marine heatwaves in

the western south Atlantic. Geophysical Research Letters, 48(22): e2021GL094509, doi: 10.1029/2021GL094509
Darmaraki S, Somot S, Sevault F, et al. 2019. Future evolution of marine heatwaves in the Mediterranean Sea. Climate Dynamics, 53(3): 1371–1392, doi: 10.1007/s00382-019-04661-z
Di Lorenzo E, Mantua N. 2016. Multi-year persistence of the 2014/15 North Pacific marine heatwave. Nature Climate Change, 6(11): 1042–1047, doi: 10.1038/nclimate3082
Dong Tianyun, Liu Fei, Dong Wenjie, et al. 2023. Double intensification centers of summer marine heatwaves in the South China Sea associated with global warming. https://www.research-square.com/article/rs-2536963/v1[2023-02-02/2023-05-17]
Eakin C M, Sweatman H P A, Brainard R E. 2019. The 2014–2017 global-scale coral bleaching event: Insights and impacts. Coral Reefs, 38(4): 539–545, doi: 10.1007/s00338-019-01844-2
Eyring V, Bony S, Meehl G A, et al. 2016. Overview of the coupled model intercomparison project phase 6 (CMIP6) experimental design and organization. Geoscientific Model Development, 9(5): 1937–1958, doi: 10.5194/gmd-9-1937-2016
Feng Yuting, Bethel B J, Dong Changming, et al. 2022. Marine heatwave events near Weizhou Island, Beibu Gulf in 2020 and their possible relations to coral bleaching. Science of the Total Environment, 823: 153414, doi: 10.1016/j.scitotenv.2022.153414
Frölicher T L, Fischer E M, Gruber N. 2018. Marine heatwaves under global warming. Nature, 560(7718): 360–364, doi: 10.1038/s41586-018-0383-9
Frölicher T L, Laufkötter C. 2018. Emerging risks from marine heat waves. Nature Communications, 9(1): 650, doi: 10.1038/s41467-018-03163-6
Gleckler P J, Taylor K E, Doutriaux C. 2008. Performance metrics for climate models. Journal of Geophysical Research: Atmospheres, 113(D6): D06104, doi: 10.1029/2007jd008972
Han Tongxin, Xu Kang, Wang Lijuan, et al. 2023. Extremely long-lived marine heatwave in South China Sea during summer 2020: Combined effects of the seasonal and intraseasonal variations. Global and Planetary Change, 230: 104261, doi: 10.1016/j.gloplacha.2023.104261
Hayashida H, Matear R J, Strutton P G, et al. 2020. Insights into projected changes in marine heatwaves from a high-resolution ocean circulation model. Nature Communications, 11: 4352, doi: 10.1038/s41467-020-18241-x
Hobday A J, Alexander L V, Perkins S E, et al. 2016. A hierarchical approach to defining marine heatwaves. Progress in Oceanography, 141: 227–238, doi: 10.1016/j.pocean.2015.12.014
Hobday A J, Oliver E C J, Sen Gupta A, et al. 2018. Categorizing and naming marine heatwaves. Oceanography, 31(2): 162–173, doi: 10.5670/oceanog.2018.205
Holbrook N J, Scannell H A, Sen Gupta A, et al. 2019. A global assessment of marine heatwaves and their drivers. Nature Communications, 10: 2624, doi: 10.1038/s41467-019-10206-z
Holbrook N J, Sen Gupta A, Oliver E C J, et al. 2020. Keeping pace with marine heatwaves. Nature Reviews Earth & Environment, 1(9): 482–493, doi: 10.1038/s43017-020-0068-4
Hughes T P, Kerry J T, Álvarez-Noriega M, et al. 2017. Global warming and recurrent mass bleaching of corals. Nature, 543(7645): 373–377, doi: 10.1038/nature21707
Liu Kai, Xu Kang, Zhu Congwen, et al. 2022b. Diversity of marine heatwaves in the South China Sea regulated by ENSO phase. Journal of Climate, 35(2): 877–893, doi: 10.1175/jcli-d-21-0309.1
Ministry of Agriculture of the People's Republic of China. 2017. Notice of the Ministry of Agriculture on printing and distributing the national marine ranching demonstration zone construction plan (2017– 2025) (in Chinese). https://www.gov.cn/gongbao/content/2018/content_5277757.htm [2017-10-31]
Oliver E C J, Benthuysen J A, Darmaraki S, et al. 2021. Marine heatwaves. Annual of Review Marine Science, 13: 313–342, doi: 10.1146/annurev-marine-032720-095144
Oliver E C J, Burrows M T, Donat M G, et al. 2019. Projected marine heatwaves in the 21st Century and the potential for ecological impact. Frontiers in Marine Science, 6: 734, doi: 10.3389/fmars.2019.00734
Oliver E C J, Donat M G, Burrows M T, et al. 2018. Longer and more frequent marine heatwaves over the past century. Nature Communications, 9: 1324, doi: 10.1038/s41467-018-03732-9
O'Neill B C, Tebaldi C, Van Vuuren D P, et al. 2016. The scenario model intercomparison project (ScenarioMIP) for CMIP6. Geoscientific Model Development, 9(9): 3461–3482., doi: 10.5194/gmd-9-3461-2016
Pearce A F, Feng Ming. 2013. The rise and fall of the "marine heat wave" off Western Australia during the summer of 2010/2011. Journal of Marine Systems, 111/112: 139–156,doi: 10.1016/j.jmarsys.2012.10.009
Plecha S M, Soares P M M. 2020. Global marine heatwave events using the new CMIP6 multi-model ensemble: From shortcomings in present climate to future projections. Environmental Research Letters, 15(12): 124058, doi: 10.1088/1748-9326/abc847
Plecha S M, Soares P M M, Silva-Fernandes S M, et al. 2021. On the uncertainty of future projections of Marine Heatwave events in the North Atlantic Ocean. Climate Dynamics, 56(7): 2027–2056, doi: 10.1007/s00382-020-05529-3
Qiu Zijian, Qiao Fangli, Jang C J, et al. 2021. Evaluation and projection of global marine heatwaves based on CMIP6 models. Deep Sea Research Part II: Topical Studies in Oceanography, 194: 104998, doi: 10.1016/j.dsr2.2021.104998
Reynolds R W, Smith T M, Liu Chunying, et al. 2007. Daily high-resolution-blended analyses for sea surface temperature. Journal of Climate, 20(22): 5473–5496, doi: 10.1175/2007jcli1824.1
Smale D A, Wernberg T, Oliver E C J, et al. 2019. Marine heatwaves threaten global biodiversity and the provision of ecosystem services. Nature Climate Change, 9(4): 306–312, doi: 10.1038/s41558-019-0412-1
Smith K E, Burrows M T, Hobday A J, et al. 2021. Socioeconomic impacts of marine heatwaves: Global issues and opportunities. Science, 374(6566): eabj3593, doi: 10.1126/science.abj3593
Song Qianghua, Yao Yulong, Wang Chunzai. 2023. Response of future summer marine heatwaves in the South China Sea to enhanced western Pacific subtropical high. Geophysical Research Letters, 50(14): e2023GL103667, doi: 10.1029/2023GL103667
Sun Xuerong, Ge Fei, Fan Yi, et al. 2022. Will population exposure to heat extremes intensify over Southeast Asia in a warmer world?. Environmental Research Letters, 17(4): 044006,doi: 10.1088/1748-9326/ac48b6
Tan Hongjian, Cai Rongshuo, Wu Renguang. 2022. Summer marine heatwaves in the South China Sea: Trend, variability and possible causes. Advances in Climate Change Research, 13(3): 323–332, doi: 10.1016/j.accre.2022.04.003
Tang Cong, Shi Jian, Zhang Yu, et al. 2023. Changes and mechanisms of long-lived warm blobs in the northeast pacific in low-warming climates. Journal of Climate, 36(7): 2277–2292, doi: 10.1175/JCLI-D-22-0152.1
Xiao Fuan, Wang Dongxiao, Leung M Y T. 2020. Early and extreme warming in the South China Sea during 2015/2016: Role of an unusual Indian Ocean Dipole event. Geophysical Research Letters, 47(17): e2020GL089936, doi: 10.1029/2020gl089936
Xue Jingyuan, Shan Haixia, Liang Junhong, et al. 2023. Assessment and projections of marine heatwaves in the Northwest Pacific based on CMIP6 models. Remote Sensing, 15(12): 2957, doi: 10.3390/rs15122957
Yang Xiaoling, Zhou Botao, Xu Ying, et al. 2021. CMIP6 evaluation and projection of temperature and precipitation over China. Advances in Atmospheric Sciences, 38(5): 817–830, doi: 10.1007/s00376-021-0351-4
Yao Yulong, Wang Chunzai. 2021. Variations in summer marine heatwaves in the South China Sea. Journal of Geophysical Research: Oceans, 126(10): e2021JC017792, doi: 10.1029/2021jc017792
Yao Yulong, Wang Chunzai, Fu Yao. 2022. Global marine heatwaves and cold-spells in present climate to future projections. Earth's Future, 10(11): e2022EF002787, doi: 10.1029/2022EF002787
Yao Yulong, Wang Junjie, Yin Jianjun, et al. 2020. Marine Heatwaves in China's marginal seas and adjacent offshore waters: past, present, and future. Journal of Geophysical Research: Oceans, 125(3): e2019JC015801, doi: 10.1029/2019jc015801
Zhou Botao, Wen Q H, Xu Ying, et al. 2014. Projected changes in temperature and precipitation extremes in China by the CMIP5 multimodel ensembles. Journal of Climate, 27(17): 6591–6611, doi: 10.1175/jcli-d-13-00761.1